Physics – Uspekhi **53** (6) 577 – 593 (2010) © 2010 Uspekhi Fizicheskikh Nauk, Russian Academy of Sciences

INSTRUMENTS AND METHODS OF INVESTIGATION PACS numbers: **07.35.+k, 62.50.–p, 64.30.–t**

Dynamic compression of hydrogen isotopes at megabar pressures

R F Trunin, V D Urlin, A B Medvedev

DOI: 10.3367/UFNe.0180.201006d.0605

Contents

Abstract. We review the results of shock compression of solid protium to the pressure 66 GPa, of liquid deuterium to 110 GPa, and of solid deuterium to 123 GPa in explosive devices of spherical geometry. The results are compared with data obtained by US scientists using traditional energy sources (explosives and light-gas guns), striker acceleration in a strong magnetic field (Z facility at Sandia), and powerful lasers (Nova at Lawrence Livermore National Laboratory (LLNL) and Omega at the Laboratory for Laser Energetics, University of Rochester). Results of density measurements of hydrogen isotopes under quasi-isentropic compression are analyzed. The absence of an anomalous increase in density under shock and quasi-isentropic compression of hydrogen isotopes is demonstrated. On the other hand, both processes exhibit a sharp change in the compression curve slopes, at the respective pressures 45 and 300 GPa.

1. Introduction

The interest in a number of high-pressure and high-temperature properties of hydrogen, including its thermodynamic properties, stems from its rich abundance in nature and applications in various technical high-power devices. For example, adequate wide-range equations of state (EsOS) of hydrogen are required for modeling the structure and evolution of stars and giant planets of the Solar System, and for calculations of the properties of highly compressed high-temperature plasma in the matter of controlled thermonuclear fusion and so on. However, regardless of the relative simplicity of hydrogen, we still do not have reliable first-principles computational models which would adequately reproduce its thermodynamic properties in the condensed state; this is mostly the result of difficulties in unambiguously taking into account the interparticle interaction, the complexities in the degeneration effects in strongly nonideal plasma, and some other factors.

In view of this, it is relevant to obtain reliable experimental data that would serve as a basis for working out semiempirical wide-range equations of state for hydrogen and as a testing material for theoretical models.

In the present review we draw most attention to analyzing precision data on the shock compression of hydrogen isotopes at maximum parameters that are available with today's explosive measuring devices. We also discuss the results of studying the dynamic compression of hydrogen under conditions of relatively gradual growth in pressure — the so-called quasi-isentropic compression under which heating is considerably lower than under shock compression.

To begin with, we shall briefly outline the chronology of experimental research into shock compression. The first measurements with liquid protium (H_2) were carried out in the USA in 1966 [1]. This was followed by publications [2, 3] in 1980 and 1983. The maximum values of parameters reported in these works corresponded to the pressure $P \approx 10$ GPa. The first results for compression of liquid deuterium (D_2) were published in 1973 [4], and measurements of Refs [2, 3] were later added to this. The maximum pressure reached in Refs [2, 3] was ≈ 23 GPa. Facilities with high explosives (HEs) and so-called light-gas guns were used as power sources for shock waves in these experiments.

No experimental research on the shock compression of hydrogen isotopes was conducted at the time in the USSR, as it had been assumed that the already available experimental data, including the results on quasi-isentropic compression [5–7], were sufficient for the determination of the hydrogen EOS parameters.

R F Trunin, V D Urlin, A B Medvedev Russian Federal Nuclear Center 'All-Russian Research Institute of Experimental Physics', 607190 Sarov, Nizhny Novgorod region, Russian Federation
Tel. (7-831-30) 2 01 27. E-mail: root@gdd.vniief.ru

Received 29 September 2009, revised 13 January 2010
Uspekhi Fizicheskikh Nauk **180** (6) 605 – 622 (2010)
DOI: 10.3367/UFNr.0180.201006d.0605
Translated by V I Kisin; edited by A Radzig

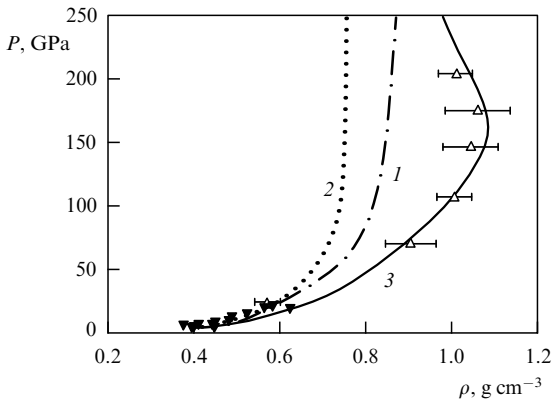

Figure 1. Data on shock compression of liquid deuterium (known in 1988). The results of experiments [2–4] — ▼, [8, 9] — △; calculated data: [10, 11] — curve *1*, [12] — curve *2*, and [8, 9] — curve *3*.

In 1997–1998, a team of researchers at the Livermore laboratory (LLNL) in the USA published the results of experiments [8, 9] on the compression of initially liquid deuterium by strong shock waves generated by the radiation of the Nova powerful laser facility. Anomalously high compression was detected at pressures above ≈ 50 GPa. Several experimental points from the results of Refs [8, 9] are plotted in Fig. 1. This figure also shows calculated adiabats of liquid deuterium from the EOS of Refs [10, 11] and appropriate equation [12] from the SESAME EOS library (USA). The first feature to catch the eye is the large discrepancy between calculations and experiments [8, 9] in the range of pressures above 50 GPa. Notice also that the curves as such are significantly different. Figure 1 also plots the calculated curve from Ref. [8] built using the model EOS in Ref. [13].

The unusual features of the Nova data caused serious doubts both in this country and abroad. V E Fortov, actively supported by R I Il'kaev, suggested testing the results of Refs [8, 9] using the shock wave generators of the Russian Federal Nuclear Center 'All-Russian Research Institute of Experimental Physics' (VNIIEF in *Russ. abbr.*). Through efforts of W J Nellis our work on liquid deuterium also received the support of the leaders of the Livermore laboratory.

To evaluate the 'scale of calamity' one had to deal with, let us consider the characteristic values of kinematic parameters encountered in such experiments: wave velocity D, and mass velocity U. As follows from a comparison of the data of Refs [8, 9] plotted on the $D-U$ coordinates with the results of linear extrapolation of the shock adiabat of liquid deuterium into the megabar pressure range [2–4], the corresponding curves at $D \approx 25$ km s^{-1} ($P \approx 90$ GPa) are at a distance of 8% in mass velocity units. Hence, if we wish to prove the validity of a specific result, the velocity measurement error must be brought substantially below 8%.

To gain additional certainty that the results are correct, it would be desirable to obtain adiabats of not only the liquid but also the initially solid phases of protium and deuterium. Joint analysis of such data would provide a better foundation for answering the question of whether anomalous compressibility develops in the megabar pressure range.

At about the same time, American researchers at the Sandia National Laboratories began checking the Nova data (in experiments with initially liquid deuterium) [14, 15]. To produce the required pressures, they used the facility in which a strong magnetic field was applied to accelerate a planar metal plate to velocities that lead to producing megabar pressures in deuterium.

It will be shown in Section 4.1 that the results obtained at the two laboratories (VNIIEF and Sandia) are in good agreement.

The results of the shockwave compression of initially liquid deuterium in the range from 45 to 230 GPa (D G Hicks et al. [16]) became known to us only after the present paper was prepared for publication. High pressures were produced in specimens by shockwaves from high-power radiation at the Omega laser facility. Compression parameters were measured in Ref. [16] just as in all our studies, by reflection technique [17]. This work confirms that there is no density jump on the shock adiabat of deuterium, in contrast to results reported using the Nova facility at a pressure of ≈ 50 GPa.

The first results of the investigation of the quasi-isentropic compressibility of protium at VNIIEF in a wide range of megabar pressures were published in 1972 [5]. Later on, some of these results were updated [6, 7, 11]. The maximum pressure implemented in these studies (still unsurpassed) amounted to ≈ 1.3 TPa (1300 GPa), the density was ≈ 2 g cm^{-3}, and the degree of compression was approximately 200. Roughly at the same time, a single measurement of the quasi-isentropic compression of hydrogen was announced in Ref. [18]. In recent years, new papers have been published in this field [19–22]; together with works [5–7, 11], they provide important data for undertaking a joint analysis of experimental data.

The paper outline is as follows. We shall discuss the results of quasi-isentropic experiments in Sections 4 and 5 after describing the data on shockwave compression in Sections 2 and 3. In Section 6 we shall give the results of representing the experimental data by two distinct semiempirical models of the equation of state.

2. Selection of shockwave compression measuring devices and their characterization

2.1 SC hemispherical measuring devices

In order to ensure independent checking of the Nova data, it would be desirable to run it on devices that create shock waves not by laser action but, for example, utilizing high explosives. Among such devices used at VNIIEF and based on accelerating impactors by the explosion products, a spherical device known as a 'soft charge' (SC or MZ in *Russ. abbr.*) [23] produced parameters of state close to those implemented at the Nova facility.

The schematic diagram of the SC is shown in Fig. 2. The hemispherical HE charge is initiated at the same time across the outer surface of the hemisphere using a special lens systems. The products of the explosion of the overcompressed detonation wave generated in the process expand as they propagate across a narrow air clearance and accelerate — relatively smoothly — the shell-impactor made of low-carbon steel of grade St-3 (because this steel consists essentially of pure iron, and their densities coincide, we make no distinction between these materials). As the wave converges toward the center, the velocity of the shell increases continuously, and in some SC devices at small radii reaches values of ≈ 23 km s^{-1}, which corresponds to megabar pressures in the initially condensed deuterium.

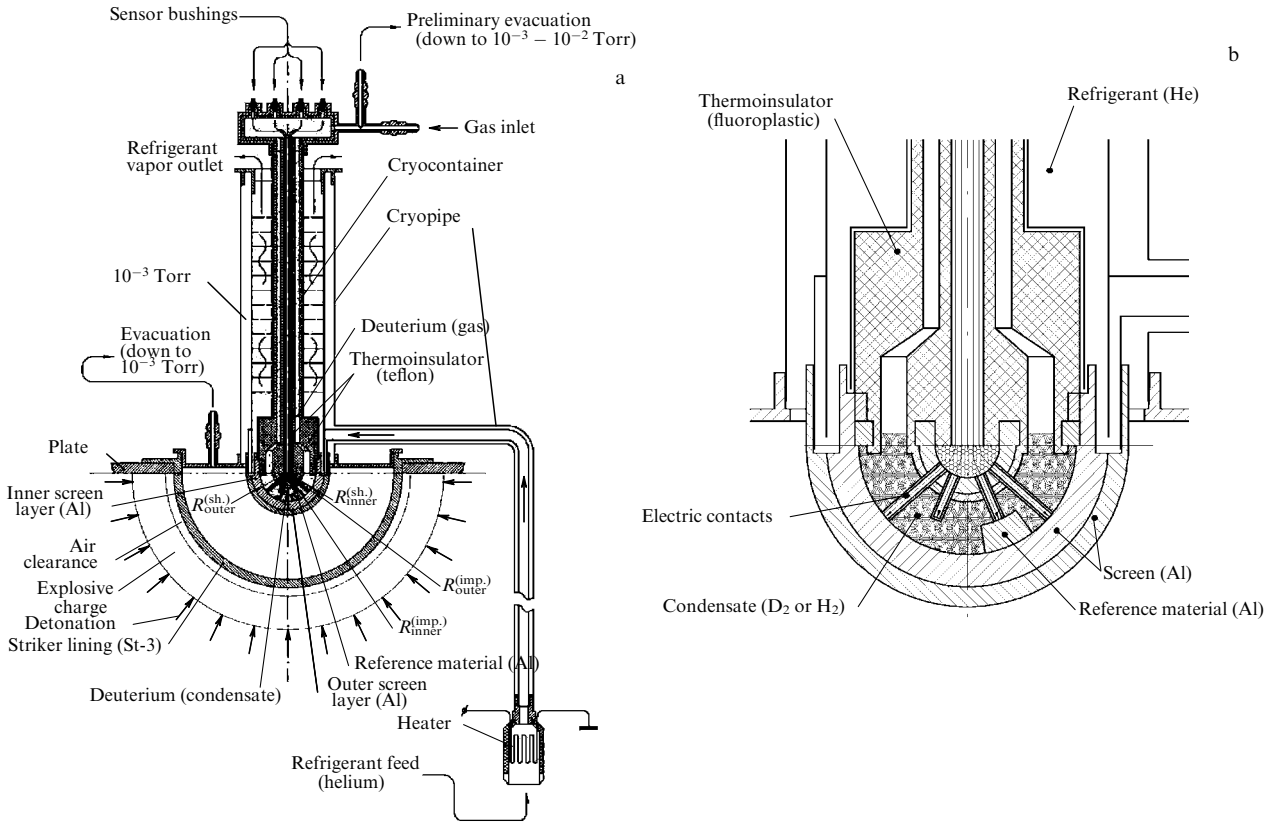

Figure 2. Schematic diagram of the experimental device: (a) general view, and (b) central part.

During the experiments, the sample is placed behind a shield made of reference material, in accordance with the reflection technique [17]. For the shield material our study used aluminum — the only metal whose shock adiabat lies relatively close to the shock adiabats of hydrogen isotopes and whose EOS is known rather well. Besides — and this is important — unloading isentropes of Al calculated from a number of its recent semiempirical equations of state differ insignificantly; this permits determination of mass velocities in deuterium at acceptable accuracy. Other, 'softer' substances, in particular alkali metals or alkali-earth metals whose Hugoniots are located closer on the pressure scale to the shock adiabats of deuterium and protium, cannot be used as shield material since they have been investigated in much less detail compared to Al and are technologically unfriendly owing to their high chemical activity.

Three designs of soft charges were selected (seven in all were designed): MZ-4, MZ-8, and MZ-18.

In MZ-4 and MZ-8 charges, the steel hemispherical shell of thickness $\Delta_{imp} = 3.08$ mm was initially located at a radius $R^{ext}_{imp} = 77$ mm. In the MZ-18 charge, $\Delta_{imp} = 3$ mm and $R^{ext}_{imp} = 130$ mm.

In MZ-4, the outer screen radius was $R_{scr} = 35$ mm, thickness of double-layer screen $\Delta_{scr} = 4$ mm (1 mm + 3 mm), average measured radius $R_m = (R_2 + R_1)/2 = 29$ mm, gauge length (specimen thickness) $S = R_2 - R_1 = 4$ mm, where R_2 and R_1 are the outer and inner radii of the reference and investigated specimens, respectively, and R_2 coincides with the inner radius of the screen.

In MZ-8, $R_{scr} = 24.1$ mm, $\Delta_{scr} = 4.5$ mm (1.5 mm + 3 mm), $R_m = 17.6$ mm, and $S = 4$ mm.

In MZ-18, $R_{scr} = 23$ mm, $\Delta_{scr} = 6.5$ mm (2.5 mm + 4 mm), $R_m = 14.5$ mm, and $S = 4$ mm. The HE radius in this device was larger than the HE radius in the former two by a factor of 1.4.

Estimates of the actual compression parameters in liquid deuterium showed that pressure produced with the MZ-4 charge can reach ≈ 30 GPa, which is not very far from the pressure built up in experiments with initially liquid deuterium [2–4]. The measurements were conducted to confirm the agreement with measurements carried out with HE SCs in Refs [2–4], particularly in order to correctly cover the effects (see Section 2.2) caused by the nonstationary nature of converging waves.

Estimates of pressure produced in deuterium in the MZ-8 (≈ 60 GPa) and MZ-18 (≈ 100 GPa) charges agreed with the characteristics achieved in the Nova experiments.

Deuterium and protium, which were initially in the solid state, were also investigated using the MZ-4, MZ-8, and MZ-18 measuring devices.

Note the following advantage of SC systems in comparison with laser facilities: the opportunity to study relatively thick samples (approximately 20 times thicker than specimens used in Refs [8, 9]). To a certain extent this eliminates the possible influence of the nonuniformity of the laser beam on the formation of waves at the interface between the screen and the analyzed hydrogen isotope, which could affect the measurements of wave characteristics in thin samples.

2.2 Specificity of measurements using spherical explosive devices

The main recorded parameter in the experiments in question is the time of travel of the shock waves in investigated and reference samples. At a known thickness of the samples (the measurement base), the corresponding velocities of travel of

shock waves across the samples can be used as the experimental parameters.

Using spherical systems for studying compression phenomena involves certain factors. The major ones are as follows

(1) There is a difference between the average velocity $D_{av} = S/\Delta t$ obtained from experiments and the local ('instantaneous') shock wave velocity at the same measurement radius R_m. The difference between them, $\Delta D_1 = D_{loc} - D_{av}$, is found by comparing the average and local velocities at R_m from the corresponding calculated curve of the wave transmission (obtained by simulating the real geometry of the gas-dynamics problem). The obtained value of ΔD_1 taking into account the calculated difference between D_{av} and D_{loc} is then added to the experimentally found value of D_{av}. In the case of deuterium, the magnitude of ΔD_1 proved to be negligibly small. For protium, ΔD_1 was slightly higher, but here too it generally did not exceed a few tenths of a percent.

(2) There is a discrepancy between the radius of measurement of wave velocities and the radius of the interface between the aluminum screen and the substance under investigation. We know that the parameters of the reference (Al) and investigated substances (D_2 or H_2) need to be compared at their interface ('at the discontinuity'), where the condition of equality of pressures and mass velocities holds in both substances. However, the known values are the experimental parameters of the transmitted wave in the reference Al and in D_2 (or H_2) at the radius R_m which differs from the radius of the contact boundary by half the thickness of the sample, $S/2$. Therefore, the next improvement in the results involves 'transferring' the actual hydrogen–screen interface to the radius R_m. The corresponding correction ΔD_2 to the experimental quantity D_{av} is introduced from a comparison of calculated velocities in the material under investigation in the actual geometry of the experiment and in the modified geometry in which the hydrogen–screen interface has been moved over the radius R_m. In this particular case, the correction, whose absolute value is at most 1.5%, is positive (it should be added to the local velocity).

(3) Finally, we should point to yet another feature of measurements in SC systems. The asymmetry of the convergence of shock waves in an investigated sample in zones of independent recording of the quantities (there are three such zones in each experiment; see Section 3) comes to about 50 ns, with the total asymmetry in the measurement zone being $\leqslant 100$ ns. As the range of experimentally covered time intervals was 140–270 ns, this necessitated that series of 3 to 5 experimental runs be conducted to obtain correct results at each experimental point in the shock adiabat of the substance being investigated.

Let us also have a closer look at the important question concerning the interpretation of experimental data, namely how to use the expansion isentrope of Al, starting from the states in the shock adiabat produced in Al at the radius R_m (each soft charge corresponds to one such isentrope). Recall that the states of hydrogen we are after are determined by the intersection of this isentrope with the wave ray $\rho_0 D$ of hydrogen. The Al isentrope is calculated from its EOS. The question is which of the equations of state of aluminum (there are several) should be used for the calculation of these isentropes.

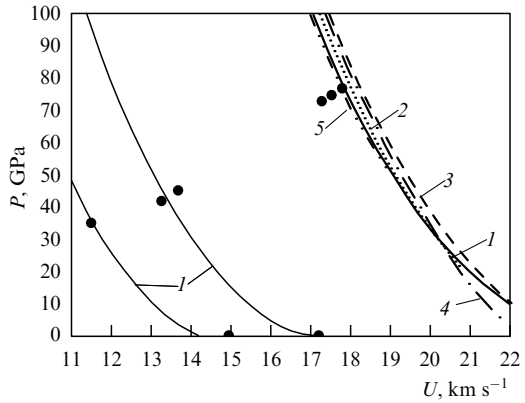

Figure 3. Expansion isentropes of aluminum: ● — experimental data [14, 29]; calculated isentropes based on EOS: [24] — *1*, [25] — *2*, [26] — *3*, [27] — *4*, and [28] — *5*.

Figure 3 plots isentropes calculated from five equations of state of Al [24–28], which best conform with the totality of experimental data. All the equations of state describe the data on shock compression of aluminum just about equally well; in fact, there is very little experimental data in the region of the $P-U$ diagram of interest to us, suitable for testing the EOS parameters, except shockwave parameters. Three experimental points are known, reported by American researchers for isentropic expansion of aluminum from the initial pressures of 500, 300, and 240 GPa [14] in the shock adiabat of Al up to relatively low pressures corresponding to the shock adiabat of low-density silicon aerogel (points in Fig. 3 at $\approx$ 75, 42, and 35 GPa). We also know the parameters of several points in the isentropes of Al as it expands into air [29].

A comparison of model isentropes of Al, calculated for various EsOS in Fig. 3, was carried out at the same initial pressure ($\approx$ 500 GPa) in the Al shock adiabat. In any close description of the Al shock adiabat by each of the considered EOS, there is a noticeable difference in the location of model isentropes.

This difference is greatest for the initial states in the $P \approx 700$ GPa adiabat of aluminum, roughly corresponding to 110 GPa in deuterium. In this case, the maximum difference in the mass velocity U is $\approx 3\%$ (for the isentrope of Ref. [27] and for that of Ref. [28] U equals 17.7 and 18.3 km s^{-1}, respectively).

Figure 3 demonstrates that the equation of state deduced in Ref. [24] corresponds to the data of experiments with aerogels somewhat better than others of the compared EOS for Al. Therefore, this equation was chosen as preferable for the interpretation of experiments with hydrogen [24]. This has also taken into account that the position of the isentrope of Ref. [24] practically coincides with the position of the isentrope of Ref. [28], which was chosen for the interpretation of similar experiments in the USA.

Notice that the isentrope of Ref. [25] is also close to the isentrope of Ref. [24], e.g., the difference between the positions of the isentropes [24] and [25] on velocity axis U is $\approx 1\%$ at the initial pressure of 720 GPa in the shock adiabat of aluminum (maximum pressure in Al when using the MZ-18 device) and at pressures 65 and 115 GPa (at which the maximum parameters of compression of protium and deuterium have been measured, respectively) .

The selected equation of state of Al [24] was applied both to determine the parameters of state in the screen, and in gas-

dynamics calculations of material flows in all measuring devices. The parameters of compression of hydrogen isotopes obtained using other equations of state for Al will differ slightly from those given in the present paper (within 2–3% in U), although this distinction is not critical for the conclusions concerning shockwave compression of the isotopes studied.

3. Experimental setup for measuring shock compression

3.1 Sensors and their location when registering shock waves

We used electrical pin contactors (sensors) prepared as bifilar twisted copper wire coated with an insulating layer of varnish (10 μm thick). The initial turn of the wire is the operating point of the sensor. For strictly fixing the sensor in space, it is placed in a miniature nickel tube (with diameter $\leqslant 0.8$ mm). The voltage applied to the sensor is 300–500 V. The grounded body of the tube serves as the second electrode. The shock wave arriving at the pin destroys the insulating layer, causing electrical breakdown, so that the registering device records a corresponding time mark. The simplicity and reliability of this sensor, applied in practical dynamic measurements for several decades now, were the main reasons for choosing it. We also took into account that just such electrical pin contactors were used in previous measurements on the parameters of shock waves on selected explosive charges (with other substances).

Our experiments used the so-called plug arrangement (Fig. 4) in which three specimen plugs for investigation are placed above the screen symmetrically in relation to the vertical line (traced by a dash-and-dot line in Fig. 4); Fig. 4 shows one of the Al specimens. This is the traditional arrangement of the samples in 'hemispherical' (and 'planar') experiments: the vast majority of measurements followed this placement mode [29]. The traditional scheme has a number of advantages over other methods of placement of samples (e.g., in the form of a segment or full hemisphere). It should be noted that in many cases the parameters of screens, especially those made of light elements, including Al, were earlier determined precisely in the 'plug' version of placement of specimens and contacts. It was therefore desirable, for the sake of compatibility with earlier arrangements (with respect to the initial states), to ensure, short of complete copying of the measurement unit (the composition and initial density of HE, the diameters of the plugs, the angle of their placement, etc.), at least the preservation of a geometry which would be close to the previous one.

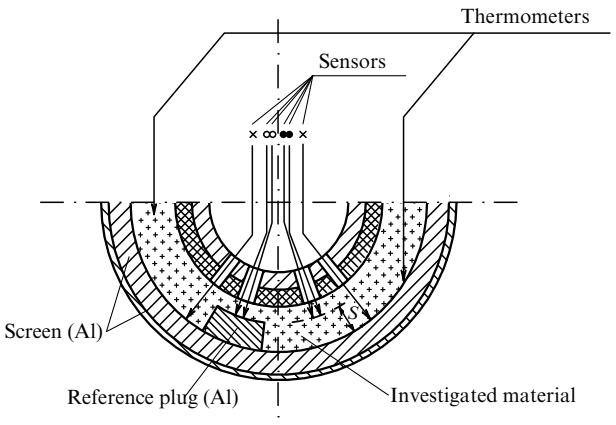

Figure 4. Longitudinal section of the measuring cell. The figure shows the Al plug. The substance under investigation (D_2 or H_2) occupies the entire remaining area marked with cruciate hatching. In this area two plug zones to be investigated are placed; their placement is symmetrical relative to the Al plug, and the placement of measurement sensors is the same as the placement of sensors on the Al plug. The locations of electrical pin contactors and thermometers are shown by arrows. The arrows with diagonal crosses indicate the locations of sensors on the inner surface of the screen (four sensors distributed evenly around each plug). They record the instant of time when the shock waves emerge from the screen into the investigated substance. Arrows with hollow circles indicate the positions of the sensors recording the arrival of the wave at the end of the measurement zone (S) in Al, and arrows with dark circles indicate the positions of the sensors recording the arrival of the wave at the end of the measurement zone in deuterium (protium).

States in the aluminum screen of the MZ-18 explosive charge were not determined at an earlier stage, so it was necessary to find them. It was natural to combine these measurements with recording velocities directly in deuterium (hydrogen). This could be done only in a plug version of the placement of specimens — otherwise, twice as many experiments would have to be conducted.

The experimental times of travel of shock waves through each specimen were calculated as the difference Δt between the readings of sensors mounted on the specimen (upper contacts) and averaged readings of sensors mounted on the screen and surrounding the sample (lower contacts). Working signals from sensors were recorded by HP54645D and TDS5254B oscilloscopes.

It is known that to obtain reliable parameters for shock compression of the substance under study in such systems it is necessary to conduct several experiments and then average their results. Typically, 3 to 5 separate experiments are sufficient for obtaining correct data. Note that results are defined as 'correct' in the sense that this number of experiments (and hence the number of plugs of the substance under study) results, as a rule, in a mean-square error of the arithmetical mean of not greater than 1–2% of the wave velocity. We adhered to this criterion both in experiments discussed in Section 4 and in all our previous studies, for any of the charges used.

3.2 The system of condensation and temperature control

A special cryogenic device for the transfer of deuterium (protium) from the gas phase to the condensed state, developed by G B Boriskov and A I Bykov with colleagues [30], was described in detail in Refs [30, 31–35] and successfully applied in all experiments to measure the shock compression of hydrogen isotopes. This device provides a gradual cooling of the measuring cell containing the gas of a tested isotope by liquid helium (and its vapor) to temperatures necessary for the condensation of the gas. The appropriate technological process permits regulation of the amount of incoming helium for cooling and thereby allows one to maintain the resulting condensate within the required temperature and time intervals.

Typically, when specimens of hydrogen in the initial liquid state were studied, the temperature of the gas-filled measuring chamber was maintained constant (after the chamber cooled down to the desired level of about 22 K) over the period (about 20 min) required for the preparation and detonation of the measuring explosive charge.

When working with initially solid specimens, a two-stage temperature regime was implemented: the specimen was first

Table 1. The parameters of shock compression of deuterium*.

Parameters of Al reference plug**		Device	ρ_0, g cm^{-3}	D, km s^{-1}	U, km s^{-1}	P, GPa	ρ, g cm^{-3}
D, km s^{-1}	U, km s^{-1}						
21.15	12.53	MZ-18	0.171	28.87 ± 0.40	22.05 ± 0.30	109 ± 3	0.724 ± 0.060
21.15	12.53	MZ-18	0.199	28.65 ± 0.40	21.59 ± 0.40	123 ± 2	0.808 ± 0.060
16.39	8.53	MZ-8***	0.171	$\mathbf{28.38 \pm 0.30}$	$\mathbf{15.38 \pm 0.20}$	$\mathbf{53.6 \pm 1.0}$	$\mathbf{0.697 \pm 0.050}$
16.39	8.53	MZ-8	0.199	20.51 ± 0.20	15.06 ± 0.15	61.5 ± 0.9	0.749 ± 0.030
13.29	5.99	MZ-4	0.171	15.25 ± 0.30	10.95 ± 0.20	28.6 ± 0.8	0.606 ± 0.040
13.29	5.99	MZ-4	0.199	15.34 ± 0.30	10.76 ± 0.20	32.8 ± 0.9	0.667 ± 0.050

* Wave velocities in deuterium and protium (Tables 1 and 2, respectively) are given with corrections for the differences between the mean (experimental) wave velocities and the 'instantaneous' values (over the measurement radius). The differences between measurement radii and the radii of the Al–D_2 (or Al–H_2) boundary were also taken into account. The total correction ($\Delta D_1 + \Delta D_2$) comes to $\approx +50$ m s^{-1} for MZ-4, $\approx +70$ m s^{-1} for MZ-8, and $\approx +175$ m s^{-1} for MZ-18.

** The parameters of the initial states in the aluminum reference plug in Tables 1 and 2 refer to the adiabat of the initially 'cold' Al (initial temperature $T_0 \approx 15$ K).

*** Parameters in bold were for the first time discussed at the 6th Zababakhin's Scientific Session in 2001 [36].

Table 2. The parameters of shock compression of protium*.

Parameters of Al reference plug		Device	ρ_0, g cm^{-3}	D, km s^{-1}	U, km s^{-1}	P, GPa	ρ, g cm^{-3}
D, km s^{-1}	U, km s^{-1}						
21.15	12.53	MZ-18	0.088	31.30 ± 0.30	23.82 ± 0.30	65.6 ± 1.0	0.368 ± 0.030
16.39	8.53	MZ-8	0.088	22.20 ± 0.50	16.43 ± 0.30	32.1 ± 0.9	0.339 ± 0.030
13.29	5.99	MZ-4	0.088	16.67 ± 0.30	11.59 ± 0.20	17.0 ± 0.3	0.289 ± 0.020

* See footnotes to Table 1.

kept for 5–10 min in the sustainable liquid state, then cooled to the solid phase (5–10 K for protium, and 5–15 K for deuterium), and remained at this temperature until the explosive charge was detonated.

Strict adherence to the specified temperature regime was the condition for producing the liquid or solid initial state of the isotope required in the test program.

Monitoring the temperature of cooled specimens was achieved by using miniature (characteristic dimension of about 1 mm) semiconductor resistance thermometers, which provided the determination of temperatures near the desired values with an error not exceeding 2% of the measured value.

4. Measurement data

The parameters obtained for the shock compression of deuterium and protium are listed in Tables 1 and 2.

Discussion of experimental results for shock compression. Of the three types of initial states of investigated specimens (solid H_2, liquid D_2, and solid D_2), the best scrutinized was liquid deuterium. The data for it were obtained in plane-wave experiments [2–4] (using HEs and gas guns), in spherical systems with an acceleration of liner-impactors by converging products of explosion [31–33, 35], and also in new systems using laser [8, 9, 16] and electrodynamic [14, 15] devices. The results of experiments with initially liquid and solid deuterium plotted on the $D-U$ coordinates are shown in Fig. 5. Notice first of all the good agreement of our data for liquid deuterium with the results of Sandia Laboratories [14, 15] in almost the entire range of recorded velocities. A good match is also observed for the parameters of the 'lowest' experimental point received in the MZ-4 device, and the data [2–4] at relatively low pressures. As we have mentioned, the aim of measurements with this explosive charge was to confirm the correctness of low-density measurements of the compression of condensed matter, in this case — condensed hydrogen isotopes, on hemispherical and flat measuring devices by comparing them. The coincidence of the experimental point for liquid deuterium with the data of American researchers obtained for plane geometry removes this issue.

The experimental points for liquid D_2 obtained at the Nova facility, beginning with $D \geqslant 17$ km s^{-1}, do not coincide with the new D vs. U curve obtained at the VNIIEF and Sandia Laboratories (curve *1* in Fig. 5). The slopes of the adiabats also greatly differ. A specific test substance being characterized by so vastly different experimental findings had never happened before in dynamic measurements. It should be emphasized that the results given in the present paper cannot be brought into agreement with the Nova results by

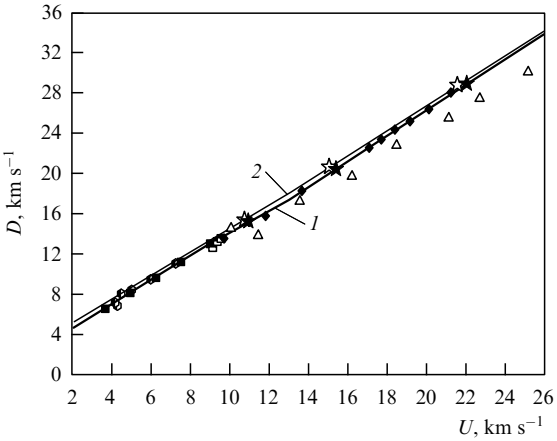

Figure 5. The data on shock compression of initially liquid and initially solid deuterium on the $D-U$ coordinates. The experiment with liquid D_2: ◐ — [2], ■ — [3], ⬒ — [4], △ — [8, 9], ◆ — [14, 15], ★ — [35]. The experiment with solid D_2: ☆ — [35]. Approximation of experimental data for D_2: curves *1* and *2* represent the liquid and solid initial states, respectively.

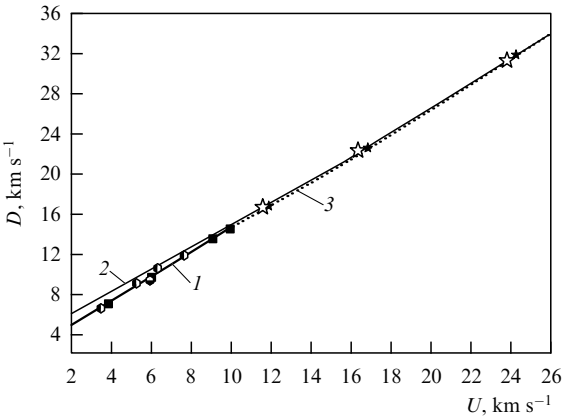

Figure 6. Data on shock compression of protium on the $D-U$ coordinates. Experiment with liquid H_2: ◒ — [1], ◐ — [2], ■ — [3]. Experiment with solid H_2: ☆ — [34]. Approximation of experimental data for H_2: *1* and *2* — liquid and solid initial states, ★ — points for liquid protium, calculated from experimental data for solid protium; *3* — approximation of calculated data for liquid protium.

any reasonable (i.e., falling within measurement errors) variations of parameters in explosion experiments.

Two Hugoniots obtained for deuterium in the liquid and solid initial states (see Fig. 5) and the adiabat of the initially solid protium (Fig. 6) are in reasonable agreement. In $D-U$ variables, the data for the initially solid H_2 ($\rho_0 = 0.88$ g cm^{-3}) and the solid ($\rho_0 = 0.199$ g cm^{-3}) and the liquid ($\rho_0 = 0.171$ g cm^{-3}) D_2 can be approximated by roughly parallel curves that are close to each other and which are then characterized by qualitatively identical features.

Let us consider them using liquid deuterium as an example. The deuterium adiabat can be described in the first approximation by three linear segments:

$$D = C_0 + sU\,.$$

The first section (up to $U \leqslant 9$ km s^{-1}) corresponds to the data of Refs [2, 4] and thus to $C_0 = 2.2$ km s^{-1}, $s = 1.20$. In the second section (9 km s^{-1} $\leqslant U \leqslant$ 13 km s^{-1}), $C_0 = 3.2$ km s^{-1}, $s = 1.09$. In the third section (13 km s^{-1} $\leqslant U \leqslant$ 30 km s^{-1}), $C_0 = 0.8$ km s^{-1}, $s = 1.27$.

Already the representation of the curve $D(U)$ in the form of a broken line consisting of three linear segments at unequal slopes is an unusual one, rarely encountered in the practice of researching shock adiabats. Other representations are also possible, of course, for example, a cubic description of the second segment like that in Ref. [33] with a parabolic description of the first segment, but this does not lead to a drastic change (we prefer the simplest description). The representation of the adiabat in the form of three segments with sharply distinct slopes should have certain physical causes. In this case, the most probable cause appears to be the dissociation of hydrogen molecules, i.e., the transition of the substance to the atomic state.

To carry out a data analysis (based on the formulas for an ideal gas) which would extend the analysis started in Ref. [33], look at the slopes of the adiabat in the second and third segments. Figure 5 shows that the slope s of the adiabat of liquid deuterium at the bend point joining the second and third segments increases appreciably (by about 14%). Let us turn to analyzing the variation in the effective thermal Grüneisen coefficient Γ in the selected segments of the adiabats of liquid deuterium and to its connection to the dissociation process that occurs during the compression of deuterium. By definition, the coefficient Γ defines the ratio of thermal pressure to thermal energy density: $\Gamma = (1/\rho)(\partial P/\partial E)_\rho$. The temperature of the compressed matter increases with increasing amplitude of the shock wave, and thermal energy is redistributed between particles with different degrees of freedom. For monatomic gases, with only translational degrees of freedom, we have $\Gamma = 2/3$. For a gas constituting a mixture of diatomic molecules and atoms formed as a result of their dissociation, we obtain, after taking into account rotational and vibrational degrees of freedom of the molecule, the expression [37]: $\Gamma = 2(1+\beta)/(7-\beta)$, where β is the degree of molecular dissociation. In the range of ultimate compression, one has $\Gamma = 2/(\sigma_{\lim} - 1)$ [for the linear $D(U)$ function], with $\sigma_{\lim} = s/(s-1)$. In this case, $\Gamma = 2(s-1)$ and, given the relation between Γ and β, we obtain $s = 8/(7-\beta)$. In the absence of dissociation, one finds $\beta = 0$, $\Gamma = 2/7$, $\sigma_{\lim} = 8$, $s = 1.14$. After the dissociation is completed, it is readily shown that $\beta = 1$, $\Gamma = 2/3$, $\sigma_{\lim} = 4$, $s = 1.33$.

The experiment indicates that in the third region (40 GPa $\leqslant P \leqslant$ 100 GPa) $s \approx 1.27$, which corresponds to $\sigma_{\lim} \approx 4.7$, $\Gamma \approx 0.54$, and $\beta \approx 0.7$. Most of the molecules in these conditions appear to be dissociated. The value of $s \approx 1.20$ in the first pressure range ($P \leqslant 20$ GPa) corresponds to $\beta \approx 0.3$, i.e., in this range only a relatively small number of molecules are dissociated. A comparison of the estimates of β in the first and third segments of the adiabat shows that in the second pressure range (20 GPa $\leqslant P \leqslant$ 40 GPa) an intense process of D_2 thermal dissociation probably occurs. This approximate analysis is also confirmed by the results of model calculations [11, 38] which suggest that the dissociation process behind the shock wave front starts for $P \geqslant 20$ GPa, at a temperature of about 5000 K (this coincides with the lower boundary of the second segment), and ends mostly at pressures of about 40–50 GPa, at a temperature of about 15,000 K. The initial point of the third segment of the $D(U)$ curve corresponds to approximately the same pressures ($U \approx 15$ km s^{-1}, $D \approx 20$ km s^{-1}, $P \approx 50$ GPa). These estimates do not contradict the data of Refs [15, 38–41], either. The Hugoniots of solid protium (see Fig. 6) and solid deuterium (see Fig. 5), as well as the Hugoniot of liquid deuterium, can be represented on the $D-U$-coordinates by linear segments. Notice that all adiabats have nearly the same slope (in fact, the difference between slopes falls within the measurement errors). Hence it follows that the above estimates of the Grüneisen coefficient and of the degree of molecular dissociation are valid for all three adiabats.

Consider the experimental data plotted on the $P-\rho$ coordinates. We have already mentioned that to obtain reliable data on the compression of substance in each spherical measuring SC device, it is necessary to conduct a series of 3 to 5 separate experiments and then average the results. This is illustrated in Fig. 7 which depicts, in addition to mean values (stars), points for individual experiments (circles and squares) with solid deuterium (MZ-8 and MZ-18 devices). The parameters for each of the two groups of points were obtained at different but fixed initial states in the aluminum screen. Substantial difference in the position of points for individual experiments is obvious (it grows even larger when errors in the screen are taken into account).

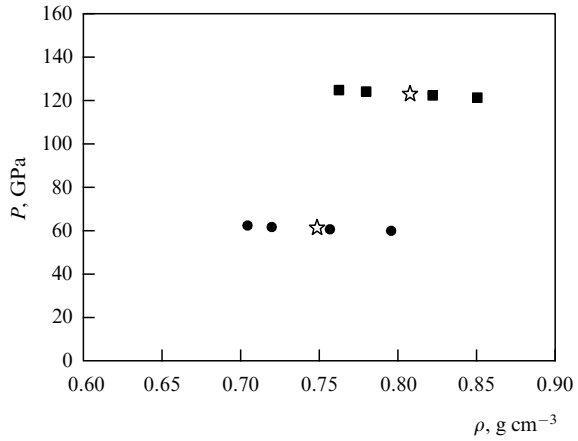

Figure 7. The results of individual shockwave experiments with solid deuterium on the $P-\rho$ coordinates: ■ — MZ-18 device, ● — MZ-8 device, and ☆ — averaged results of statistical processing.

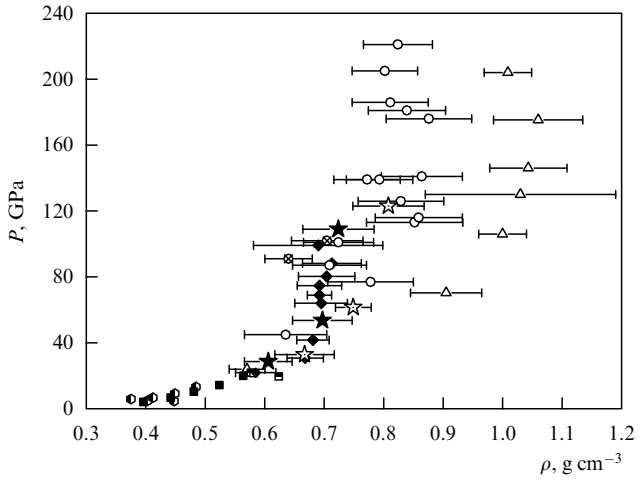

Figure 8. Data on shock compression of deuterium on the $P-\rho$ coordinates. The notation is similar to that in Fig. 5, with the following exceptions: ○ — [16], and ⊗ — [43].

Therefore, a completely unrealistic picture of the compression of matter can be produced if the study is limited to working with isolated measurements of shock compression.

All results for deuterium are compared in Fig. 8. Here, we see especially clearly the contradiction between the Nova data and the results obtained in this work and at Sandia Laboratories. It has been suggested [42] that a possible reason for the sharp increase in density in Refs [8, 9] could be the nonstrict maintenance of geometry of the experiment relating the direction of propagation of the shock wave created by a laser beam and the direction of roentgenographic recording of the wave parameters in deuterium that should be perpendicular to it. This could lead to overestimation of the mass velocity and, hence, to increased compression. As evident from Fig. 8 (see also Ref. [33]), mutual errors of the approximating curves caused by the aggregate error of all our experimental points and the data of Ref. [15] do not overlap with the Nova data (taking into account their own errors). At the same time, their mutual coincidence is rather satisfactory. We also need to emphasize the consistency of the results on shock compression of the two phases of hydrogen isotopes, obtained by a technique repeatedly tested in several hundred independent experiments, including experiments with gas guns and explosives. All this is convincing proof of the fallacy of the results reported in Refs [8, 9].

Figure 8 also presents recently published data on the shock compression of initially liquid deuterium at pressures of up to 230 GPa [16], obtained using the Omega laser facility. Despite the relatively large experimental 'spread' in the positions of individual experimental points (representing individual experiments), the new data on the whole agree with the results found in Refs [14, 15, 33, 35] (in the investigated common range of pressures $P \leqslant 100$ GPa) and at the same time contradict the results obtained at Nova facility [8, 9]. The data of Ref. [16] for pressures above 110 GPa deflect from a smoothly extrapolated curve towards higher densities. Their position corresponds to a maximum possible compression of about 5.

This figure also presents two experimental points for deuterium reported in Ref. [43], which were obtained with the MZ-18 explosive device; the design of the measurement cell was modified in comparison with the one described in the present paper. The experiments utilized gaseous deuterium compressed at an initial pressure of 150 and 200 MPa (densities equal to 0.133 and 0.153 g cm^{-3}). To retain the gas in the ampule at such high initial pressure, it was necessary to use KhN35VTYu high-strength alloyed steel ('lined' on its inner cavity surface with aluminum) as the load-bearing envelope of the screen. One experiment was run with deuterium for each of the above initial density values. As we mentioned earlier, a single experiment is decidedly insufficient for obtaining a representative set of data on hemispherical measurement systems. Hence, the credibility of information generated in these experiments is not high. The positions of the experimental points themselves are good evidence of this (see Fig. 8); for instance, deuterium compression parameters with $\rho_0 = 0.153$ g cm^{-3} coincide at equal pressures with the parameters of condensed deuterium ($\rho_0 = 0.171$ g cm^{-3}).

It would undoubtedly be useful to have data on the compression of lower-density deuterium at megabar pressures. Hopefully, the authors of Ref. [43] will be able to carry out the necessary number of fully-fledged experiments to achieve this goal.

The results of experiments on shock compression of the originally solid protium, plotted on the $P-\rho$ coordinates, are shown in Fig. 9, where they are compared with data of Refs [1–3], which represent the liquid initial state at significantly lower pressures. Arrows indicate the estimated positions of the experimental points normalized to the initial density $\rho_0 = 0.071$ g cm^{-3} (density of the initially liquid protium).

Such normalization for protium was carried out with small linear extrapolation of the $D(\rho)$ straight lines to the density of its liquid state, $\rho_0 = 0.071$ g cm^{-3}. On the whole, we received satisfactory agreement between Russian and U.S. data for liquid protium. It should be noted that no one up to the present has studied the shock compression of protium in the originally solid state.

5. On the quasi-isentropic compression of hydrogen

To date, experimental results have been published on measuring the quasi-isentropic compression of protium and deuterium under dynamic conditions, obtained by three

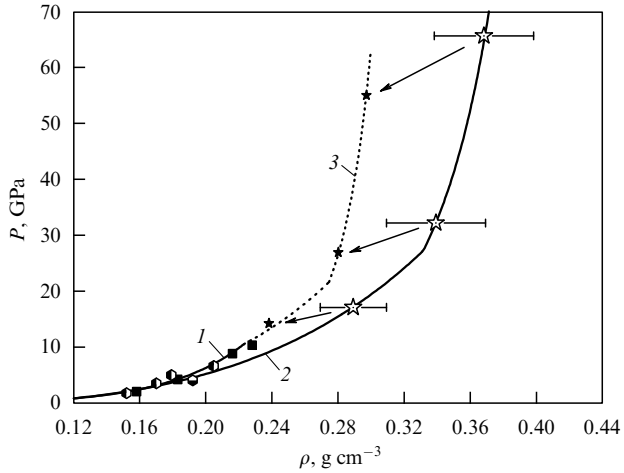

Figure 9. Shock compression of protium: data plotted on the $P-\rho$ coordinates. Notation is the same as shown in Fig. 6.

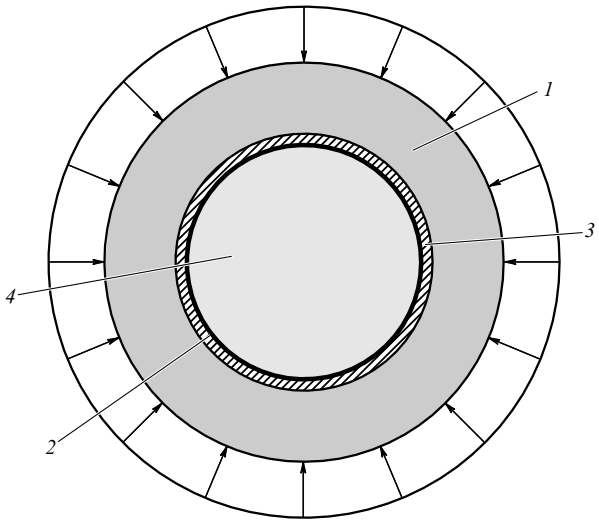

Figure 10. Schematic diagram of experiments for studying quasi-isentropic compression of hydrogen using spherical devices: *1* — explosive, *2* — contrasting foil, *3* — steel shell-impactor, *4* — gas to be studied.

groups of researchers at VNIIEF — [5–7, 11], [19–21], and [22]. There is also a publication by American scientists from LLNL [18]. Note, however, that publication [18] was of a methodological nature and that the estimates of hydrogen compression presented in it were treated as preliminary (e.g., the calculated values of hydrogen pressures at close range of density measurements could vary from 100 to 300 GPa). Unfortunately, the authors of Ref. [18] have not published their final results.

In works [5–7], the authors investigated gaseous protium at an initial temperature of 323 K. The initial values of pressure, density, and entropy (in units of the gas constant R) are given in Table 3. The experiments used a test design with a spherical geometry (Fig. 10) containing an explosive layer detonated simultaneously over the outer surface, a steel shell in close proximity to the explosive layer, and a contrasting heavy-metal envelope whose inner cavity was filled with the protium to be investigated. After the explosion of the charge, the products of the explosion accelerated the shell, which was decelerated by the gas as the shell moved toward the center. The trajectory of the shell motion until it stopped (this instant of time corresponds to the maximum compression of the gas) and reverse movement from the center began was recorded on photographic films in a series of experiments using the transmitting X-ray emission from a powerful X-ray facility; the film was kept in a protective holder. The average density of compressed hydrogen is determined by the diameter of the inner cavity at a fixed instant of time, and by the initial mass of gas. A direct result of the experiments is a set of curves for the radius R of the inner shell as a function of time t. Each of the functions $R(t)$ corresponds to a certain initial size of the shell compressing the gas, and the initial gas pressure (density) in the cavity. Papers [5–7] give, along with the experimental values of the maximum (in fact averaged) hydrogen density ρ, the calculated values of the mean pressure P corresponding to a given density ρ. Pressure was found from calculations of wave gasdynamic processes in the experimental device. In order to find the pressure, an averaging procedure was applied to the layer containing about 80% of the mass of the compressed gas (variability of pressure distribution in the gas could be as high as 10 to 20%). During pressure computations, equations of state of all substances included in the measurement system were used, including the EOS of protium itself. Protium's parameters were varied in such a way that all the experimental curves $R(t)$ were faithfully reproduced (data from other independent experiments, including those characterizing the properties of hydrogen under static loading conditions, were also involved to determine the model EOS). Notice that it has been shown in comparative experiments performed with hydrogen and deuterium that the two isotopes had equal compressibility.

An important aspect is the determination of the effect of selecting the equations of state of the substances and the computation algorithms on the adequacy of the description of gasdynamic motion of the shell in the absence of gas in the cavity (i.e., the dynamics of the piston compressing the gas). A special series of experiments demonstrated agreement between calculated and experimental parameters at the stage

Table 3. Parameters of the quasi-isentropic state.

The initial values of parameters at $T = 323$ K			The values of parameters at the instant the shell stops			
P_0, MPa	ρ_0, g cm^{-3}	S/R	$r_{\min}$, mm	ρ, g cm^{-3}	P, GPa	T, K
75	0.0390	9.4	29.0 – 30.4	0.42 – 0.48	38	1800
160	0.0635	8.6	22.8 – 23.6	0.64 – 0.70	110	2000
100	0.0470	9.1	19.1 – 20.3	0.90 – 1.06	320	2800
75	0.0390	9.4	17.0 – 18.0	1.04 – 1.26	340	3300
50	0.0292	9.8	14.5 – 15.5	1.26 – 1.54	490	3700
25	0.0164	10.5	11.2 – 12.0	1.54 – 1.90	870	5200
15	0.0104	11.0	9.1 – 10.1	1.70 – 2.30	1300	7000

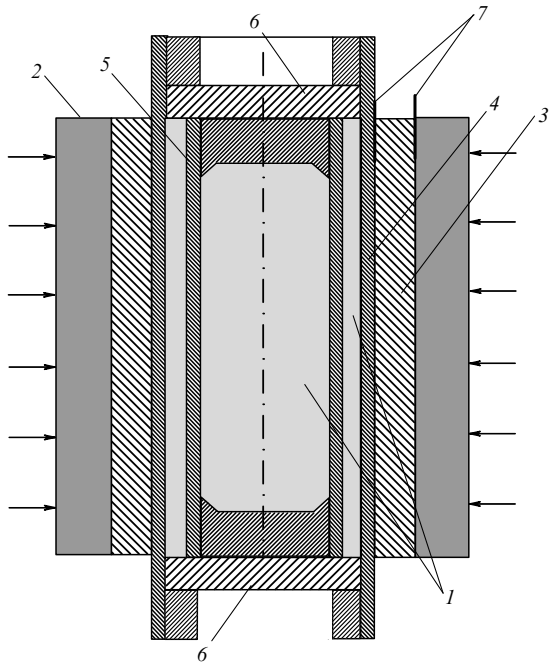

Figure 11. Cylindrical geometry of experiments: *1* — gas, *2* — explosive, *3* — plexiglas spacer, *4*, *5* — steel shells, *6* — blank flanges, *7* — electrical pin contactors.

of convergence of the shell without gas; they also pointed to the possibility of studying the EOS of hydrogen isotopes in the selected experimental design.

The initial values of pressure (published in Ref. [5]) were to some extent corrected in subsequent publications by the same team of researchers [6, 7, 11] (partly due to refinements in the protium EOS). One value of average density ρ (at $P \approx 800$ GPa), for which by mistake a wrong value was given in Ref. [5], has also been corrected. The data after final processing were presented in Ref. [11] (see Table 3 where calculated values of the mean P and T are given alongside the experimental values of ρ for protium).

It should be emphasized that the process of hydrogen compression in the experiments [5] (and similar ones) is of a complex wave nature. It starts with the gas compression by a shock wave with an amplitude of $\approx 1.5-3$ GPa (subsequent waves are characterized by substantially lower amplitudes). The 'post-compression' of the gas to the actually averaged density is produced by a superposition of waves reflected from the center and from the shell moving toward the center. Under this relatively slow compression, the gas is heated substantially less than in compression by a strong shock wave at the same final pressure. This technique maintains the quasi-isentropic nature of the process. The calculated protium temperature in these experiments [11] was estimated as $\approx 1800-7000$ K (the lowest values of T correspond to $P \approx 38$ GPa, and the largest to $P \approx 1300$ GPa).

The design selected in Refs [19–21] used an explosive cylindrical device in which the steel shell of the internal cascade compressed gaseous deuterium via a mitigating cushion of the same gas. Schematic diagram of the experiment can be seen in Fig. 11. The initial density of deuterium was 0.04 g cm^{-3}. Just as in work [5], the final results in Refs [19–21] are the number of experimental values of the average density ρ and the calculated values of the mean pressure P at the instant the shell expansion in the second cascade stops (the calculation of P used the EOS of Ref. [10] with the parameters chosen in such a way that the results of calculations with them were consistent with the experimental results obtained in Ref. [5]). A comparison of data on quasi-isentropic compression of protium [5–7, 11] and deuterium in Refs [19–21] was carried out assuming that the ratio of their densities in the isobars equalled two. Estimates of the final temperature of deuterium (several thousand kelvins) are on the same order of magnitude as in Ref. [11].

The images of compressed gas in both types of devices were obtained using the roentgenographic recording technique. Unfortunately, the image quality decreases as pressure grows. This is best seen at pressures starting from 100–150 GPa. According to our estimates, the accuracy of recording density under these conditions is never better than $\approx$ 15–20%. Approximately the same error (20%) is also typical of the calculated values of pressure (mostly because of the variability of pressure when the shell stops expanding). The cause of large density errors seems to reflect the instability of the shell flight, particularly shell separation into layers at the above-mentioned pressures ($\geqslant 100-150$ GPa). At any rate, a number of photographs at high pressures show stratification quite clearly. The obvious consequence is loss of accuracy in determining the radius when the shell stops, i.e., the density of the gas.

The data on quasi-isentropic compression of initially solid deuterium and protium (at an initial temperature of $\approx$ 5 K) by a metal shell accelerated by a strong magnetic field produced by the MK-1 generator were published in conference proceedings [22]. A cylindrical system of compression was employed, in which the magnetic field transfers its energy to a copper shell which compresses the material to be tested. The cavity radius R was determined (as it was in Refs [5–7, 11, 19–21]) by a roentgenographic recording technique. The mean hydrogen density ρ was found by measuring the radius R determined at the moment of X-ray exposure. The mean pressure P in experiments conducted in Ref. [22], corresponding to the experimentally established ρ, was obtained not from calculations as in Refs [5–7, 11, 19–21] but from experimentally found average compression of the aluminum reference specimen located above the specimen with the hydrogen isotope. The difference between mean pressures in hydrogen and aluminum was taken into account by calculations. Therefore, two state parameters of the substance under investigation were determined in Ref. [22]: the mean ρ, and P. In contrast to the corresponding values in Refs [5–7, 11, 19–21], these values do not necessarily correspond to the maximum compression of the gas by the shell (X-ray radiography in Ref. [22] was executed at the instants of time at which the pressure differences between hydrogen and aluminum were relatively small). In principle, the multiframe mode of X-ray radiography [22] makes it possible to obtain information on the hydrogen compression in a single experiment consecutively and virtually in the entire range of pressures implemented in the experimental device in the course of compression.

Owing to a low initial temperature of the substance in the experiments carried out in Ref. [22], the finally achieved temperature was also relatively low (estimated not to exceed several hundred Kelvin degrees at maximum recorded pressures).

Figure 12 gives all available results on quasi-isentropic compression of protium and deuterium on the $P-\rho$ coordi-

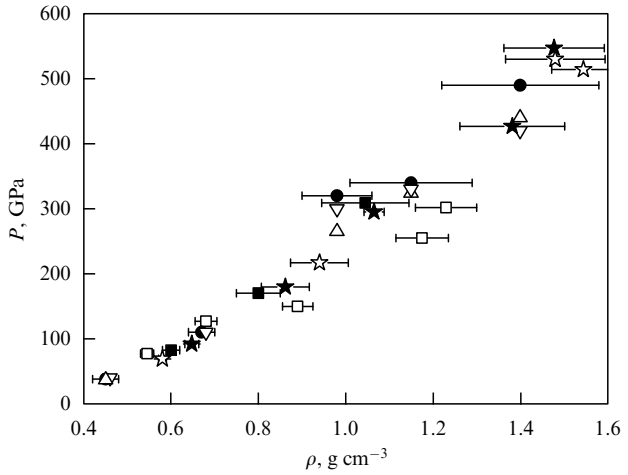

Figure 12. Quasi-isentropic compression of deuterium and protium: △ (H_2) — [5], ▽ (H_2) — [6], ● (H_2) — [7, 11], ■ (D_2) — [19, 20], □ (D_2) — [21], ★ (D_2), and ☆ (H_2) — [22].

nates (for the sake of comparison, the experimental density of deuterium was reduced by a factor of 2). The data of Refs [5–7, 11] are nonmonotonic, with compressibility behavior changing at ≈ 300 GPa, which was treated in these studies as a transition of molecular protium to the atomic state. The results of Refs [19, 20] in the first segment (up to ≈ 300 GPa) are in good agreement with those of Refs [5–7, 11]. On the whole, the results obtained in Ref. [22] do not contradict the data of Refs [5–7, 11], and this former group can also be said to point to the nonmonotonic behavior of the compression curve with changing compressibility at $P \approx 300$ GPa. Notice also that since the temperature realized in experiments [22] was lower than in Refs [5–7, 11], the substance density recorded in Ref. [22] was higher than that observed in Refs [5–7,11] (in isobars), which is quite normal.

We therefore see that, in the matter of changing hydrogen compressibility behavior at $P \approx 300$ GPa, satisfactory agreement over the totality of results found in papers [5–7, 11, 19, 20, 22] is reached.

The results presented in Ref. [21] differ essentially from all data presented above as paper [21] reports an approximately 20% jump in density at $P \approx 150$ GPa. We think that the cause of the disagreement is the overestimation by the authors of Ref. [21] of the accuracy of their results. Indeed, an analysis of their data shows that the error in the experimental determination of density and in calculations of pressure in paper [21] considerably exceeds the level given in this publication. The following fact provides evidence of this. The same group of authors as in Ref. [21] comes to a conclusion in Refs [19, 20] that their data agrees to within experimental errors with the data of work [5–7], while in the next publication [21] (without comment or citing earlier conclusions [19, 20]) they report a drastically different behavior of the isentropic compression curve.

6. Equations of state of protium and deuterium

In this section, we shall give a description of the results of experiments conducted using two different forms of the equation of state. First we consider the equation of state developed in Refs [11, 24], which reflects the behavior of matter in the solid and liquid states.

6.1 Equations of state of protium and deuterium in solid and liquid states

6.1.1 Equation of state of solid phase. The free energy of a crystalline solid is given by

$$F_{\text{solid}} = E_{\text{cold}}(\rho) + 1.125R\theta + RT\left\{3\ln\left[1-\exp\left(-\frac{\theta}{T}\right)\right] - \mathrm{D}\left(\frac{\theta}{T}\right)\right\} + F_{\text{vib rot}}(\rho, T) + F_{\text{elec}}(\rho, T)\,, \quad (1)$$

where T and ρ are temperature and density, R is the gas constant, $\theta(\rho)$ is the Debye temperature, $\mathrm{D}(x)$ is the Debye function defined as

$$\mathrm{D}(x) = 3x^{-3}\int_0^x \frac{x^3\,\mathrm{d}x}{\exp x - 1}\,.$$

The first term on the right-hand side of formula (1) corresponds to the interaction potential of molecules in the crystal, while the second and third describe the zero-point and thermal fluctuations in the crystal. The fourth and fifth terms describe the rotation and vibration of atoms, respectively, in a molecule located in the crystal lattice cell, and the thermal excitation of electrons. The following expressions proved the most suitable for practical purposes:

$$E_{\text{cold}} = \frac{3}{\rho_{\text{cr}}}\sum_i a_i\left(\frac{\delta^{i/3}-1}{i}\right),$$

$$\theta = \theta_0\delta^{1/3}\left(C_{\text{cold}}^2 - \frac{2nP_{\text{cold}}}{3\rho}\right)^{0.5},$$

where $\delta = \rho/\rho_{\text{cr}}$, $P_{\text{cold}} = \rho^2\,\mathrm{d}E_{\text{cold}}/\mathrm{d}\rho$, $C_{\text{cold}}^2 = \mathrm{d}P_{\text{cold}}/\mathrm{d}\rho$, ρ_{cr} is crystal density at $P_{\text{cold}} = 0$, and n is an empirical parameter. The four coefficients a_i in formulas for E_{cold} are also empirical parameters. Three of them are determined from the conditions imposed on the description of the density of the solid phase at zero temperature and melting temperature at atmospheric pressure, and from the known value of the binding energy. The fourth factor is determined from the condition on the description of one experimental point in the isotherm. The parameter θ_0 is obtained from the experimental value of the Debye temperature. The accepted value for hydrogen isotopes is $n = 1.5$. With this value of n, the experimental low-temperature isotherms in the solid phase are somewhat better described.

The rotational temperature of diatomic molecules involving hydrogen isotopes is significantly higher than the normal melting temperature: $\theta_{\text{rot}\,0} = 87.6$ K for H_2, and $\theta_{\text{rot}\,0} = 43.8$ K for D_2. Hence, the rotational component in the equation of state must be taken into account already when describing the melting curve. The vibrational temperature of a hydrogen molecule is significantly higher than the rotational temperature: $\theta_{\text{vib}\,0} = 6331$ K for H_2, and $\theta_{\text{vib}\,0} = 4483$ K for D_2. At high temperatures, one also needs to take into account ionization and the dissociation of molecules located at lattice sites of molecular hydrogen. Here, this component is presented in the analytical form suggested in Ref. [12], which takes into account the density dependences of dissociation and ionization energies:

$$F_{\text{vib rot}} = RT(\ln Q_{\text{vib}} - \ln Q_{\text{rot}})\,,$$

where

$$Q_{\rm vib} = \frac{1-\exp(-\omega/T)}{1-\exp(-\varphi/T)}\,,$$

$$\omega = \frac{\theta_{\rm vib}}{1+TC_T}\,, \qquad \varphi = \frac{\theta_{\rm dis}}{1+TC_T}\,, \qquad C_T = \frac{0.125\theta_{\rm vib}}{\theta_{\rm dis}^2}\,,$$

$$\theta_{\rm vib} = \theta_{\rm vib\,0}\left(\frac{\rho}{\rho_1}\right)^{G_{\rm vib}}, \qquad G_{\rm vib} = 0, 1\,,$$

$$\theta_{\rm dis} = \theta_{\rm dis\,0}\left\{1-\exp\left[2.885\left(1-\frac{\rho_{\rm d}}{\rho}\right)^{1/3}\right]\right\}^2,$$

$$Q_{\rm rot} = (1+x^2+x^3)^{1/3}\,, \qquad x = \frac{T}{\theta_{\rm rot}}\left[1-\exp\left(-\frac{\theta_{\rm dis}}{T}\right)\right],$$

$$\theta_{\rm rot} = \theta_{\rm rot\,0}\left(\frac{\rho}{\rho_1}\right)^{G_{\rm rot}}, \qquad G_{\rm rot} = 0, 1\,,$$

$\rho_1 = 0.088$ g cm^{-3}, $\rho_{\rm d} = 4$ g cm^{-3} for H_2, and $\rho_1 = 0.199$ g cm^{-3}, $\rho_{\rm d} = 8$ g cm^{-3} for D_2, and $\theta_{\rm dis\,0} = 28{,}000$ K for both isotopes.

At temperatures above 1 eV in condensed molecular hydrogen, it is necessary to take into account the contribution of the electronic component to free energy. In accordance with the band theory, this component for insulators has the form

$$F_{\rm elec} = -\frac{4kT}{\rho}\sqrt{n_{\rm p}n_{\rm n}}\left(\frac{2\pi m^* kT}{h^2}\right)\exp\left(-\frac{W}{2kT}\right),$$

where m^* is the geometric mean of the electron and hole effective masses, k and h are the Boltzmann and Planck constants, $n_{\rm p}$ and $n_{\rm n}$ stand for the orbital degeneracy in the bands, $W = W_0\ln(\rho_{\rm e}/\rho)$, and $\rho_{\rm e}$ is the density at which the energy gap closes. The choice of $\rho_{\rm e}$ is currently problematic. The value of W_0 stems from the experimental value of W at normal density. In this paper we assume $\rho_{\rm e} = 3$ g cm^{-3} for H_2, and $\rho_{\rm e} = 6$ g cm^{-3} for D_2, and $W_0 = 3.6$ eV for both hydrogen isotopes.

6.1.2 Equation of state of the liquid phase. The equation of state of the liquid phase and the method for determining its parameters taking into account the melting curve were proposed in paper [24]. Their successful application has been shown with ionic crystals, metals, and noble gases as examples. The central idea of the approach proposed in Ref. [24] is to assume that the structure and equation of state of the liquid phase near the melting curve are very close to the structure and equation of state of the crystal. This means that the elastic components in the equations for the solid and liquid phases are identical but that the equation of state for the liquid phase should have a correction describing the presence of 'holes' in the structure of this phase. The free energy of the liquid assumes the form

$$F_{\rm liq} = F_{\rm sol} - 3RT\ln\alpha(\rho, T)\,. \qquad (2)$$

Here, function $\alpha(\rho, T)$ satisfies two limiting conditions:

(1) $F_{\rm liq}$ at high temperatures transforms smoothly into the free energy of an ideal gas;

(2) jumps in entropy $\Delta S = S_{\rm liq} - S_{\rm sol}$ and specific volume $\Delta V = V_{\rm liq} - V_{\rm sol}$ at the melting point at atmospheric pressure correspond to known experimental values. To meet these conditions, the function $\alpha(\rho, T)$ is taken in the form

$$\alpha = (1+z)^{-0.5}\exp\left[b(T) - f(\sigma)\,\frac{T_0}{T}\right],$$

where

$$z = \frac{L_z RT}{C_{\rm cold}^2 - 2nP_{\rm cold}/(3\rho)}\,,$$

L_z is a constant, and T_0 is the melting temperature at $P = 0$. Limiting conditions do not impose restrictions on the functions $f(\sigma)$ and $b(\sigma, T)$. To carry out specific calculations, the two are chosen as

$$f(\sigma) = c_0 + \sum_i c_i(\sigma^i - 1)\,, \qquad b(T) = b_0 + b_1\left(\frac{T_0}{T}\right)^2,$$

where $\sigma = \rho/\rho_{\rm liq}$, $\rho_{\rm liq}$ is the density of the liquid phase at T_0, while $c_1 - c_4$ and b_0, b_1 are empirical constants which are the values of thermodynamic parameters in the melting curve at normal pressure and at one or two points at high pressure; the quantities b_0 and b_1 determine how the heat of melting depends on pressure along the melting curve. The heat capacity of the liquid at the melting point at atmospheric pressure was also taken into account. It should also be noted that the function $f(\sigma)$ effectively takes into account the emergence of 'holes' in the structure of the liquid phase and the related change in the energy of elastic interaction of atoms.

6.1.3 The equation of state of solid atomic hydrogen. Theoretical calculations of the properties of atomic hydrogen were conducted by Yu M Kagan and co-workers [47]. Here, we give the formulas they used for the energy of the elastic interaction of atoms and zero-point oscillation (ZPO) energy as functions of density with the parameters calculated in the same paper:

$$E_{\rm cold}(\rho) = a_{\rm a0} + a_{\rm a1}x^2 + a_{\rm a2}x + a_{\rm a3}x^{-1} + a_{\rm a4}x^{-2} + (a_{\rm a5} + a_{\rm a6}x^{-1})\ln\rho\,,$$

$$E_{\rm ZPO}(\rho) = 1.125\,R\theta = (B_{\rm a1}x^2 + B_{\rm a2}x + B_{\rm a3})x^{-0.5} + B_{\rm a4}\,,$$

where $x^3 = \rho$ [g cm^{-3}].

The solid and liquid atomic hydrogen are described by equations (1) and (2), respectively (naturally, without the component $F_{\rm vib\,rot}$). When calculations are made in this section, condensed atomic hydrogen is considered to be metallic. In metals, the effect of electrons at low temperatures begins to occur in the solid phase. The electron component of free energy of the metal adopted in this article is chosen as

$$F_{\rm elec} = -1.5\,RT\eta\int_0^x \ln(\cosh x)\,{\rm d}x\,,$$

where $x = \beta_{\rm elec}T/(1.5R\eta)$, $\beta_{\rm elec}$ is the coefficient of electronic specific heat, η is the number of electrons in the conduction band per atom, and R is the gas constant. For hydrogen, one has $\eta = 1$. According to the band theory of metals, $\beta_{\rm elec} = 1.36\times10^{-4}$ J g^{-1} K^{-2} for H, and $\beta_{\rm elec} = 1.08\times10^{-4}$ J g^{-1} K^{-2} for D.

All the parameters for the solid and liquid phases of the molecular and atomic isotopes of hydrogen are given in

Table 4. Parameters of the equations of state of solid and liquid phases of molecular and atomic hydrogen — protium and deuterium.

Molecular phase*			Atomic phase**		
	H_2	D_2		H	D
ρ_{cr}, g cm^{-3}	0.1167	0.2487	a_{a0}, kJ mol^{-1}	1300	1305
n	1.5	1.5	a_{a1}, kJ mol^{-1}	1486.5	1486.5
θ_0, K s km^{-1}	73.81	87.63	a_{a2}, kJ mol^{-1}	−2535	−2535
a_1, GPa	−0.24	−0.33	a_{a3}, kJ mol^{-1}	−26.9	−26.9
a_2, GPa	2.8	3.66	a_{a4}, kJ mol^{-1}	−90.8	−90.8
a_3, GPa	−7.16	−8.99	a_{a5}, kJ mol^{-1}	−20.2	−20.2
a_4, GPa	4.6	5.66	a_{a6}, kJ mol^{-1}	−10.9	−10.9
L_z	4	3	B_{a1}, kJ mol^{-1}	49.2	49.2
b_0	0.4527	0.4271	B_{a2}, kJ mol^{-1}	−50.8	−50.8
B_1	0.05	0.03	B_{a3}, kJ mol^{-1}	−16.9	−16.9
c_0	0.4028	0.3699	B_{a4}, kJ mol^{-1}	43.0	35.2
c_1	−150.98	−143.86			
c_2	140.2	137.93			
c_3	−55	−56			
c_4	10	10			
T_0, K	13.8	18.6	T_{TP}, K	2379	2529
T_{boil}, K	20.4	23.6	ρ_{TP}, g cm^{-3}	1.0899	2.20625
$\rho_1(T = 1\text{ K})$, g cm^{-3}	0.0880	0.1990	P_{TP}, GPa	388.3	388.5
$\rho_{sol}(T = T_0)$, g cm^{-3}	0.0875	0.1965			
$\rho_{liq}(T = T_0)$, g cm^{-3}	0.0780	0.1760			
$\rho_{boil}(T = T_{boil})$, g cm^{-3}	0.0705	0.1709			
$\theta(\rho_1)$, K	105	105			

* Subscript 'boil' marks the parameters corresponding to boiling (at $P = 0.1$ MPa).
** Subscript 'TP' (triple point) marks the parameters of the triple point on the phase diagram in Fig. 16.

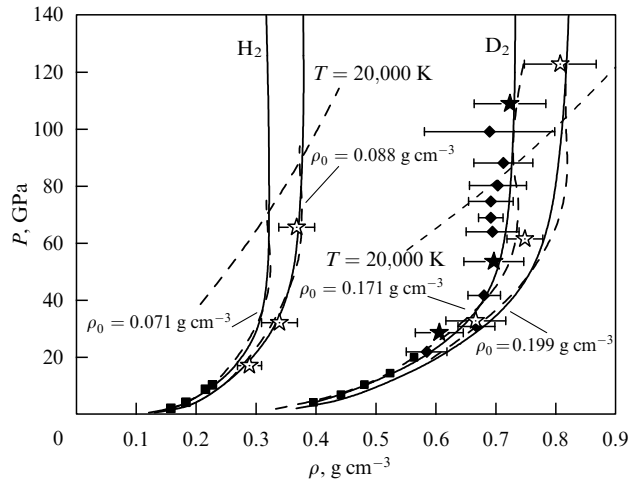

Figure 13. Shock adiabats of initially liquid and solid deuterium and protium. Solid curves give the results of calculations from the EOS of Section 6.1, and dashed curves from the EOS of Section 6.2. The isotherms for $T = 20{,}000$ K were calculated from the EOS of Section 6.2. The notation for experimental data is similar to the notation in Figs 8 and 9.

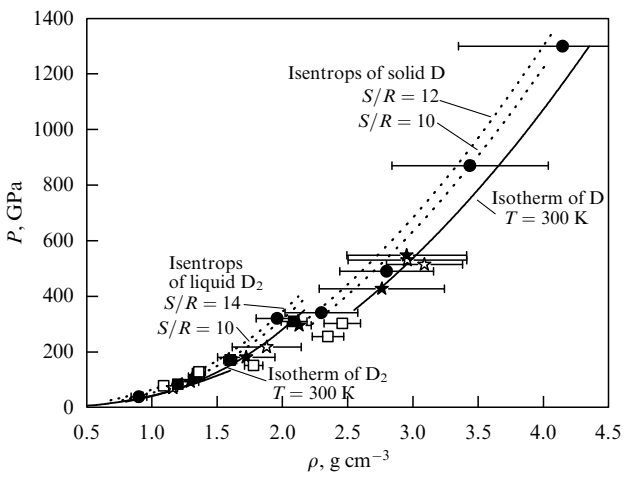

Figure 14. Isentropes and isotherms of molecular and atomic deuterium. The results of calculations using the EOS from Section 6.1. The notation of experimental data is similar to that in Fig. 12. The density of protium was increased by a factor of two. Curves fit calculated dependences. Thickened portion of the curve — an isotherm [48].

Table 4. On the basis of these characteristics, Figs 13–15 compare calculated shock adiabats, isentropes, isotherms, and the melting curve with experimental data. Satisfactory agreement is obvious, suggesting that the equation of state we

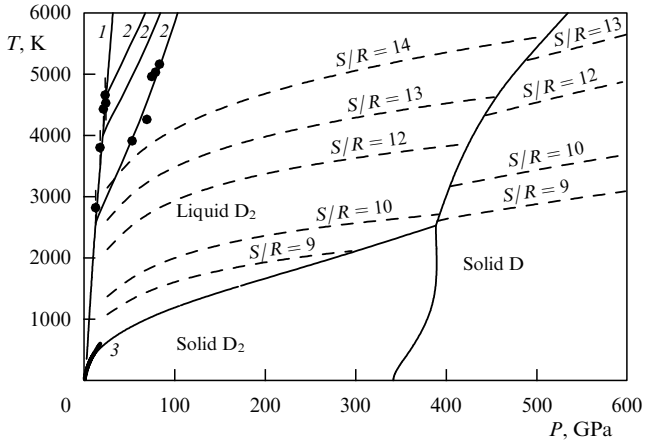

Figure 15. Phase diagram, Hugoniots, and isentropes of deuterium calculated with the equation of state of Section 6.1: *1* and *2* are a single and a doubled adiabat, ●—experimental data [3], *3*—melting curve, thickened portion of the curve—experimental data [49].

are considering allows a description of most of the thermophysical properties of hydrogen without creating contradictions.

6.2 Modified van der Waals equation of state

A modified van der Waals model (VdW) applicable also to mixtures was used for describing the experimental data on the compressibility of hydrogen isotopes [25, 45, 46, 50]. When constructing an EOS for hydrogen, the authors considered the components H_2, H, and for the EOS of deuterium, D_2, D. The model can, in principle, take into account not only dissociation but also ionization; in this context, however, the latter is ignored.

The thermal equation of state (the $P-T-V$-connection) of individual components is described in a parametric form (by introducing an additional internal variable—repulsive pressure $P^{\rm rep}$) by the following expressions:

$$P = P^{\rm rep} - a\left(\frac{N_0}{V}\right)^2, \tag{3}$$

$$P^{\rm rep} = \frac{N_0 kT}{V - V_{\rm C}}, \tag{4}$$

$$V_{\rm C} = V_{\rm C}(P^{\rm rep}), \tag{5}$$

where $N_0 = \text{const}$ is the number of particles per unit mass, and $V = 1/\rho$; k is the Boltzmann constant, and $a = \text{const}$ is the attraction parameter. The covolume $V_{\rm C}$ is an empirical function of the variable $P^{\rm rep}$ [for $V_{\rm C}(P^{\rm rep}) = \text{const}$, model (1)–(3) transforms into the original VdW model]. To express the covolume (5) in the range of states $0 < P^{\rm rep} < P_*$ ($P_* = \text{const}$ is a parameter), the following expression was employed:

$$V_{\rm C} = V_0\left[1 - \frac{\ln(P^{\rm rep}/A)}{\alpha}\right], \tag{6}$$

where V_0, A, α are empirical constants (V_0 is the effective specific volume of fluid at $T = 0$, $P = 0$). Equation (4) for $T = 0$ implies that $V = V_{\rm C}$. In this case, relations (3), (6) define the 'cold' pressure $P_{\rm cold}$ of the liquid as

$$P_{\rm cold}(V) = A\left\{\exp\left[\alpha\left(1 - \frac{V}{V_0}\right)\right] - \left(\frac{V_0}{V}\right)^2\right\}. \tag{7}$$

The derivation of formula (7) assumed that in Eqn (3) $a = AV_0^2/N_0^2$. A suitable choice of constants in formula (7) makes it possible to reflect the experimental compressibility of the liquid in the framework of model (3)–(5) in the range of moderate densities. Equation (7) becomes of little use when the density is much higher than the cryogenic value. Therefore, the following expression for $V_{\rm C}$ was utilized instead of Eqn (6) in the range $P^{\rm rep} \geqslant P_*$:

$$V_{\rm C} = B\left(\frac{P_*}{P^{\rm rep}}\right)^d + C\left(\frac{P_*}{P^{\rm rep}}\right)^f, \tag{8}$$

where B, d, C, $f = \text{const}$. The value of one of these constants (namely d) is fixed, and the others are determined from the condition of smooth matching of expressions (6) and (8) (in the values of the function $V_{\rm C}$ and its first two derivatives) for $P^{\rm rep} = P_*$. The chosen values of the parameters ($\rho_0 = 1/V_0$) for the components are given in Table 5.

Table 5. The parameters in formulas (7), (8) for protium and deuterium.

Parameter	H_2	H	D_2	D
ρ_0, g cm^{-3}	0.094	0.7	0.208	1.4
A, GPa	0.0552	40	0.0781	40
α	7.335	5	7.298	5
P_*, GPa	3.588	200	3.122	200
B, cm^3 g^{-1}	4.5926	1.8755	2.4677	0.9376
d	0.33	0.5	0.33	0.5
C, cm^3 g^{-1}	−0.00848	−0.9072	−0.08995	−0.4536
f	7.680	0.719	1.729	0.719

Free energy F corresponding to the thermal EOS (3)–(5) is determined [in its natural variables V, T jointly with formulas (4), (5)] by the expression

$$F = E^{\rm rep}(P^{\rm rep}) + E^{\rm att}(V) - N_0 kT \ln\frac{{\rm e}T^{5/2}\sigma(T)r}{P^{\rm rep}}, \tag{9}$$

where

$$E^{\rm rep} = -\int_0^{P^{\rm rep}} P^{\rm rep}\left[\frac{{\rm d}V_{\rm C}(P^{\rm rep})}{{\rm d}P^{\rm rep}}\right]{\rm d}P^{\rm rep},$$

$$E^{\rm att} = -\int_\infty^V P^{\rm att}(V)\,{\rm d}V,$$

e is the base of natural logarithms, $r = k^{5/2}[m/(2\pi\hbar^2)]^{3/2}$, m is the particle mass, $\hbar$ is the Planck constant, $\sigma(T)$ is the internal partition function of an individual particle, and $P^{\rm att} = -a(N_0/V)^2$ is the attraction pressure.

To determine $\sigma(T)$, the data relative to the reduced Gibbs potential $\Phi_0(T)$ in the $P = P_0 = 1$ atm isobar and the enthalpy of formation H_0 (at $T = 0$) of atoms and molecules were provided by handbook [51]. The function $\sigma(T)$ is related to them by the expression

$$\ln\frac{T^{5/2}\sigma(T)r}{P_0} = \frac{T\Phi_0(T) - H_0}{N_{\rm A}kT},$$

where N_A is the Avogadro constant. The range of representation of $\Phi_0(T)$ in handbook [51] is limited by the temperature $T = 20{,}000$ K.

To describe mixtures, model (4), (5), (9) is generalized as follows

$$F = E^{\text{rep}}\left(P^{\text{rep}}, \{N\}\right) + E^{\text{att}}\left(V, \{N\}\right) - kT\sum_{i=1}^{n} N_i \ln \frac{\mathrm{e}NT^{5/2}\sigma_i(T)r_i}{N_i P^{\text{rep}}}, \quad (10)$$

$$V = V_{\text{C}}\left(P^{\text{rep}}, \{N\}\right) + \frac{NkT}{P^{\text{rep}}}, \quad (11)$$

where

$$E^{\text{rep}} = -\int_0^{P^{\text{rep}}} P^{\text{rep}} \left[\frac{\partial V_{\text{C}}\left(P^{\text{rep}}, \{N\}\right)}{\partial P^{\text{rep}}}\right]_{\{N\}=\text{const}} \mathrm{d}P^{\text{rep}}, \quad (12)$$

$$E^{\text{att}} = -\int_{\infty}^{V} P^{\text{att}}\left(V, \{N\}\right)_{\{N\}=\text{const}} \mathrm{d}V. \quad (13)$$

Here, i is the number of the particle kind; n is the total number of kinds taken into account in the model (in the cases of protium and deuterium considered here, $n = 2$); N_i is the number of particles of each kind ($i = 1, \ldots, n$) per unit mass of matter; $\{N\}$ denotes the series $N_1, N_2, \ldots, N_n$ fixing the composition of the mixture, and $N = \sum_{i=1}^{n} N_i$ is the total number of particles. Expressions (10)–(13) take into account the dependence of the mixture's covolume V_{C} and attraction pressure P^{att} on the composition $\{N\}$. The integrals (12), (13) are taken for every $N_i = \text{const}$. Formulas (10)–(13) imply the expression for the pressure:

$$P = -\left(\frac{\partial F}{\partial V}\right)_{T,\{N\}} = P^{\text{rep}} + P^{\text{att}},$$

which together with formula (11) is a generalization of the thermal EOS (3)–(5).

The functions V_{C} and P^{att} in expressions (10)–(13) were found from similar characteristics of individual components using rules that proved fairly reliable when using the VdW model for mixtures [52]. For the mixture covolume, the additive expression

$$V_{\text{C}}\left(P^{\text{rep}}, \{N\}\right) = \sum_{i=1}^{n} N_i\, v_{\text{C}i}(P^{\text{rep}})$$

was used, where the covolume $v_{\text{C}i}$ refers to a single ith particle. The attraction of the mixture is given by the expression

$$P^{\text{att}} = -a_{\text{mix}}\left(\frac{N}{V}\right)^2,$$

where

$$a_{\text{mix}}^{1/2} = \frac{1}{N}\sum_{i=1}^{n} N_i a_i^{1/2}.$$

Here, a_i is a characteristic of attraction of the ith component [the quantity a on the right-hand side of formula (3)].

Equilibrium values of N_i are found (at fixed values of the variables P^{rep} and T and using balance relationships) from the equations

$$\sum_r \nu_r^l \mu_r = \sum_s \nu_s^l \mu_s,$$

where $\nu_{r(s)}^l$ are stoichiometric coefficients, l is the number of the chemical reaction, r and s are indices of the initial and the final reaction products, respectively, and $\mu_j = (\partial F/\partial N_j)_{V,T,j\neq i}$ is the chemical potential of the jth particle.

After determining the composition, the necessary thermodynamic quantities are calculated from the model formulas.

Figure 16 depicts the results of experiments on the isothermal compression of protium in the range of relatively low pressures, and data on protium evaporation [53] in comparison with the corresponding calculated values. The same satisfactory agreement between experimental and computed results was also observed for deuterium.

A comparison of the results of model calculations with the data of isothermal ($T = 300$ K) experiment [54, 55] at higher pressures is drawn in Fig. 17. The model describes the results of experiments [54, 55] in approximately the same way at temperatures below room temperature.

Figure 13 gives the experimental and calculated data on shock compression of initially liquid (at initial densities $\rho_0 = 0.071$ and 0.171 g cm^{-3}) and initially solid ($\rho_0 = 0.088$

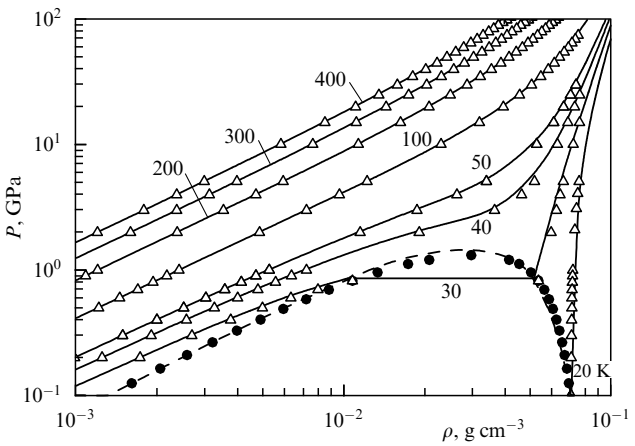

Figure 16. Pressure as a function of density along the isotherms and the liquid–vapor equilibrium curve for protium. The symbols show the data of Ref. [53], and curves plot the results of calculations (isotherms are distinguished by temperature).

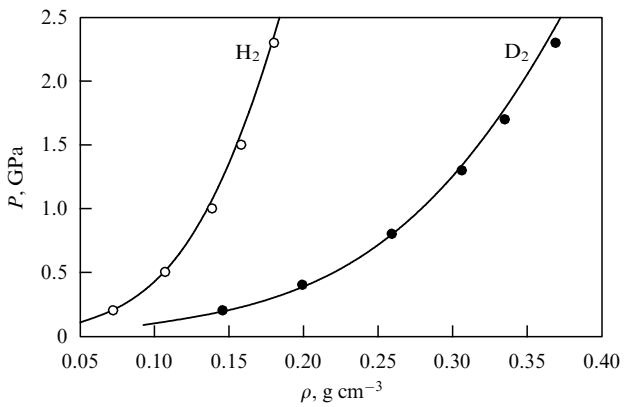

Figure 17. Isothermal ($T = 300$ K) compression of protium and deuterium. Symbols show the data of Refs [54, 55], and curves plot the results of calculations.

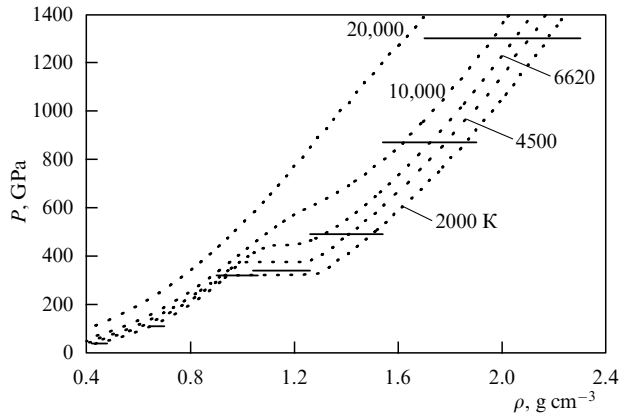

Figure 18. Data [11] on quasi-isentropic compression of protium (the length of horizontal segments reflects the error in determining the density) and model isotherms.

and 0.199 g cm^{-3}) protium and deuterium. Nonmonotonic behavior of the calculated shock adiabat is caused by dissociation.

The model described in this section was aimed at reproducing the data of Ref. [11] in the range of states studied in quasi-isentropic experiments. Figure 18 exhibits a number of model isotherms, including isotherms for $\approx$ 2000–7000 K which correspond, according to the EOS of Ref. [11], to the conditions of the quasi-isentropic experiments we discuss here. The nonmonotonic behavior of the calculated isotherms is caused by protium dissociation (a phase transition of the first order occurs below the critical point with the model parameters $T \approx 6620$ K, $P \approx 445$ GPa, and $\rho \approx 1.16$ g cm^{-3}). Model isotherms of deuterium behave in a similar manner.

As may be seen from Figs 13–18, on the whole both of the considered types of equations of state are in satisfactory agreement with the experimental data.

7. Conclusion

We shall formulate the main results outlined in this article:

• Hugoniots of initially liquid and initially solid deuterium were obtained at pressures of up to 120 GPa, as well as for solid protium at pressures of up to 66 GPa. The data for solid deuterium and protium are unique for research projects of this kind;

• the data of VNIIEF and Sandia National Laboratories do not confirm the anomalously high compressibility of deuterium discovered with the laser facility Nova at LLNL;

• slight extrapolation of the curve $D(\rho_0)$ to the density of liquid protium produced its shock adiabat in the pressure range corresponding to pressures in experiments with solid protium;

• an analysis of the results of shock compression of hydrogen isotopes showed that the more likely explanation for the obtained curves is the transition of hydrogen (deuterium) to the atomic state as a result of molecular dissociation driven by temperature and pressure in the shock wave;

• an analysis of data on the quasi-isentropic compression of protium and deuterium makes it apparent that at pressures of $\approx$ 300 GPa the slope of their compression curves changes;

• actual errors in the experimental data on quasi-isentropic compression do not support the conclusion that an abrupt change in density in the deuterium adiabat occurs at pressures of about 150 GPa;

• the description of experimental data for hydrogen isotopes using two equations of state reveals satisfactory agreement between the experimental and calculated curves under the assumptions that underlie the model calculations.

Intense work by a large team on the staff of the Institute was required for completing this research project. An important role was played at the first stage of the project (the study of shock compression of hydrogen isotopes) by G V Simakov, A N Shuikin, A Ya Matveev, S I Belov, G V Boriskov, A I Bykov, and their assistants. They were able to solve very quickly the very complicated problem of using cryogenic technology in the specific conditions of spherical explosive measuring systems and to conduct numerous complex experiments with shock compression of hydrogen isotopes. Much of the experimental data on quasi-isentropic compression was obtained by the team of S B Kormer and F V Grigor'ev in the 1970s. Many of their pioneering results remain unsurpassed for research of this caliber. The recent data obtained by the teams of Zhernokletov–Mochalov (V A Arinin, S I Kirshanov, A B Mezhevov, and some others) and Bykov–Boriskov (S I Belov, N B Luk'yanov, and some others) with systems using cylindrical acceleration of shells added essential chapters to the pioneering measurements of Kormer–Grigor'ev and made it possible to conduct an overall analysis of the results in this field. The studies of 'cold' compression of deuterium and protium conducted by the Bykov–Boriskov team, using a strong magnetic field as an energy source for shell acceleration, were especially outstanding.

The authors greatly appreciate the interest in the results of their work shown by V P Kopyshev and V V Khrustalev, as well as useful discussions with them of the theoretical aspects of the work. The authors are grateful to W J Nellis from the University of California for the useful discussions of all the experimental aspects of the project, which contributed to the successful completion of the program. O L Mikhailova, I R Trunin, I A Tereshkina, and members of their teams carried out a large amount of computational work, both for the optimization of the arrangement of experimental work and for processing the results obtained in the course of this work. L I Kanunova was extremely helpful to the authors during the preparation of the results for publication.

The work was conducted with the financial support from RFBR, project No 09-02-00375.

References

1. Van Thiel M, Alder B J *Mol. Phys.* **10** 427 (1966)
2. Dick R D, Kerley G I *J. Chem. Phys.* **73** 5264 (1980)
3. Nellis W J et al. *J. Chem. Phys.* **79** 1480 (1983)
4. Van Thiel L M et al. *Phys. Rev. Lett.* **31** 979 (1973)
5. Grigor'ev F V et al. *Pis'ma Zh. Eksp. Teor. Fiz.* **16** 286 (1972) [*JETP Lett.* **16** 201 (1972)]
6. Grigor'ev F V et al. *Zh. Eksp. Teor. Fiz.* **69** 967 (1975) [*Sov. Phys. JETP* **42** 378 (1975)]
7. Grigorev F V et al. *Zh. Eksp. Teor. Fiz.* **75** 1683 (1978) [*Sov. Phys. JETP* **48** 847 (1978)]
8. Da Silva L È et al. *Phys. Rev. Lett.* **78** 483 (1997)
9. Collins G W et al. *Science* **281** 1178 (1998)
10. Kopyshev V P, Khrustalev V V *Zh. Prikl. Mekh. Tekh. Fiz.* (2) 122 (1980) [*J. Appl. Mech. Tech. Phys.* **21** 113 (1980)]
11. Kopyshev V P, Urlin V D, in *Udarnye Volny i Ekstremal'nye Sostoyaniya Veshchestv* (Shock Waves and Extreme States of Matter) (Eds V E Fortov et al.) (Moscow: Nauka, 2000) p. 297

12. Kerley G I "Equations of state of hydrogen and deuterium", SANDIA REPORT sand 2003-3613 Unlimited Release Print (2003)
13. Holmes N C, Ross M, Nellis W J *Phys. Rev. B* **52** 15835 (1995)
14. Knudson M D et al. *Phys. Rev. Lett.* **87** 225501 (2001)
15. Knudson M D et al. *Phys. Rev. B* **69** 144209 (2004)
16. Hicks D G et al. *Phys. Rev. B* **79** 014112 (2009)
17. Al'tshuler L V, Krupnikov K K, Brazhnik M I *Zh. Eksp. Teor. Fiz.* **34** 886 (1958) [*Sov. Phys. JETP* **7** 614 (1958)]
18. Hawke R et al. *Phys. Earth Planet. Inter.* **6** 44 (1972)
19. Il'kaev R I et al., in *5-e Kharitonovskie Chteniya* (5th Khariton's Session) (Ed. A L Mikhailov) (Sarov, 2005) p. 108
20. Il'kaev R I et al. *AIP Conf. Proc.* **706** 73 (2004)
21. Fortov V E et al. *Phys. Rev. Lett.* **99** 185 (2007)
22. Boriskov G V et al. *Joint 21st AIRAPT and 45th EHPRG Intern. Conf. on High Pressure and Technology, Catania, Italy, 2007*, p. 421
23. Al'tshuler L V et al. *Usp. Fiz. Nauk* **166** 575 (1996) [*Phys. Usp.* **39** 539 (1996)]
24. Urlin V D *Zh. Eksp. Teor. Fiz.* **49** 485 (1965) [*Sov. Phys. JETP* **22** 341 (1965)]
25. Medvedev A B *Vopr. Atom. Nauki Tekh. Ser. Teor. Prikl. Fiz.* (1) 23 (1992)
26. Sapozhnikov A T, Pershina A V *Vopr. Atom. Nauki Tekh. Ser. Teor. Prikl. Fiz.* (4) 47 (1979)
27. Glushak B L et al. *Vopr. Atom. Nauki Tekh. Ser. Mat. Modelir. Fiz. Protsessov* (1) 32 (1991)
28. Kerley G I *Int. J. Impact Enging.* **5** 441 (1987)
29. Trunin R F et al., in *Eksperimental'nye Dannye po Udarno-volnovomu Szhatiyu i Adiabaticheskomu Rasshireniyu Kondensirovannykh Veshchestv* (Experimental Data on Shock-Wave Compression and Adiabatic Expansion of Condensed Matter) (Ed. R F Trunin) (Sarov: VNIIEF, 2001)
30. Boriskov G V et al., in *Intern. Conf. on Megagauss Magnetic Field Generation and Related Topics, Book of Abstracts, Nov. 5 – 10, Santa Fe, New Mexico, USA* (2006) p. 34
31. Belov S I et al. *Pis'ma Zh. Eksp. Teor. Fiz.* **76** 508 (2002) [*JETP Lett.* **76** 433 (2002)]
32. Boriskov G V et al. *Dokl. Ross. Akad. Nauk* **392** 755 (2003) [*Dokl. Phys.* **48** 553 (2003)]
33. Boriskov G V et al. *Phys. Rev. B* **71** 092104 (2005)
34. Trunin R F et al. *Pis'ma Zh. Eksp. Teor. Fiz.* **82** 317 (2005) [*JETP Lett.* **82** 284 (2005)]
35. Trunin R F et al. *Zh. Tekh. Fiz.* **76** (7) 102 (2006) [*Tech. Phys.* **51** 907 (2006)]
36. Trunin R F et al., in *6-e Zababakhinskie Nauchnye Chteniya, 2001 g.* (6th Zababakhin's Scientific Session, 2001) Report abstract; see http://www.vniitf.ru/rig/confer/6ZST/6ZST.htm
37. Zel'dovich Ya B, Raizer Yu P *Fizika Udarnykh Voln i Vysokotemperaturnykh Gidrodinamicheskikh Yavlenii* (Physics of Shock Waves and High-Temperature Hydrodynamic Phenomena) (Moscow: Nauka, 1966) [Translated into English (Mineola, NY: Dover Publ., 2002)]
38. Desjarlais M P *Phys. Rev. B* **68** 064204 (2003)
39. Celliers P M et al. *Phys. Rev. Lett.* **84** 5564 (2000)
40. Collins G W et al. *Phys. Rev. Lett.* **87** 165504 (2001)
41. Nellis W J *Phys. Rev. Lett.* **89** 165502 (2003)
42. Nellis W J et al. *Phys. Rev. B* **59** 5 (1999)
43. Grishechkin S K et al., in *7-e Kharitonovskie Chteniya* (7th Khariton's Session) (Ed. A L Mikhailov) (2005)
44. Pavlovskii A I et al., in *Sverkhsil'nye Magnitnye Polya* (Superhigh Magnetic Fields) (Eds V M Titov, G A Shvetsov) (Moscow: Nauka, 1984) p. 19
45. Kopyshev V P, Medvedev A B *Sov. Tech. Rev. B Therm. Phys. Rev.* **5** 371 (1993)
46. Medvedev A B, in *Udarnye Volny i Ekstremal'nye Sostoyaniya Veshchestva* (Shock Waves and Extreme States of Matter) (Eds V E Fortov et al.) (Moscow: Nauka, 2000) p. 315
47. Kagan Yu M, Pushkarev V V, Kholas A *Zh. Eksp. Teor. Fiz.* **73** 967 (1977) [*Sov. Phys. JETP* **46** 511 (1977)]
48. Loubeyre P et al. *Nature* **383** 702 (1996)
49. Diatschenko V et al. *Phys. Rev. B* **32** 381 (1985)
50. Medvedev A B, in *9-e Kharitonovskie Chteniya* (9th Khariton's Session) (Ed. A L Mikhailov) (Sarov, 2007) p. 318
51. Glushko V P (Ed.) *Termodinamicheskie Svoistva Individual'nykh Veshchestv* (Thermodynamic Properties of Individual Substances) Handbook (Moscow: Nauka, 1978) pp. 1–4
52. Vukalovich M P, Novikov I I *Uravnenie Sostoyaniya Real'nykh Gazov* (Equation of State of Real Gases) (Moscow–Leningrad.: Gosenergoizdat, 1948)
53. Thermophysical Properties of Fluid Systems, NIST Webbook, http://webbook.nist.gov/chemistry/fluid
54. Mills R L et al. *J. Chem. Phys.* **66** 3076 (1977)
55. Mills R L et al. *J. Chem. Phys.* **68** 2663 (1978)